Electronic Supplementary Material (ESI) for RSC Advances.
This journal is © The Royal Society of Chemistry 2014

# An enzyme-responsive supra-amphiphile constructed by pillar[5]arene/acetylcholine molecular recognition

Guocan Yu,* Jie Yang, Danyu Xia and Yong Yao

*Department of Chemistry, Department of Chemistry, Zhejiang University, Hangzhou 310027, P. R. China.*

Email address: guocanyu@zju.edu.cn.

## Electronic Supplementary Information (17 pages)

1. *Materials and methods* S1
2. *Synthesis of* ***PyCh*** S2
3. *Host–guest complexation between* ***WP5*** *and* ***M*** S8
4. *Host–guest complexation between* ***WP5*** *and* ***PyCh*** S10
5. *Critical aggregation concentration determination of* ***PyCh*** *and* ***WP5⊃PyCh*** S11
6. *Packing mode investigation of* ***PyCh*** *before and after treating with AChE* S12
7. *Preparation of supramolecular hybrid materials* S14
8. *Catalytic reduction of 4-nitroaniline* S16

*References* S17

*1. Materials and methods*

Methyl 6-bromohexanoate, 1-pyrenol, *N*,*N*-dimethylethanolamine and other reagents were commercially available and used as received. Solvents were either employed as purchased or dried according to procedures described in the literature. $^{1}$H NMR and $^{13}$C NMR spectra were recorded on a Bruker Avance Ⅲ-400 spectrometry. The 2D NOESY NMR spectrum was collected on a Bruker Avance DMX-500 spectrometer with internal standard TMS. Mass spectra were obtained on a Bruker Esquire 3000 plus mass spectrometer (Bruker-Franzen Analytik GmbH Bremen, Germany) equipped with an ESI interface and an ion trap analyzer. HRMS were obtained on a WATERS GCT Premier mass spectrometer. UV-vis spectra were taken on a Shimadzu UV-2550 UV-vis spectrophotometer. The melting points were collected on a SHPSIC WRS-2 automatic melting point apparatus. The fluorescence experiments were conducted on a RF-5301 spectrofluorophotometer (Shimadzu Corporation, Japan). Scanning electron microscopy investigations were carried out on a JEOL 6390LV instrument operating at an energy of 15 Kev or 20 Kev. Transmission electron microscopy (TEM) investigations were carried out on a HT-7700 instrument. X-ray diffraction (XRD) was recorded on a Rigaku Ultima IV instrument. The critical aggregation concentration (CAC) values were determined on a DDS-307 instrument. The ITC experiment was performed on a VP-ITC micro-calorimeter (Microcal, USA). Energy-minimized structure of **WP5⊃M** was calculated using PM3 semiempirical molecular orbital methods (Frisch, M. J.; Trucks, G. W.; Schlegel, H. B.; Scuseria, G. E.; Robb, M. A.; Cheeseman, J. R.; Montgomery, J. A., Jr.; Vreven, T.; Kudin, K. N.; Burant, J. C.; Millam, J. M.; Iyengar, S. S.; Tomasi, J.; Barone, V.; Mennucci, B.; Cossi, M.; Scalmani, G.; Rega, N.; Petersson, G. A.; Nakatsuji, H.; Hada, M.; Ehara, M.; Toyota, K.; Fukuda, R.; Hasegawa, J.; Ishida, M.; Nakajima, T.; Honda, Y.; Kitao, O.; Nakai, H.; Klene, M.; Li, X.; Knox, J. E.; Hratchian, H. P.; Cross, J. B.; Adamo, C.; Jaramillo, J.; Gomperts, R.; Stratmann, R. E.; Yazyev, O.; Austin, A. J.; Cammi, R.; Pomelli, C.; Ochterski, J. W.; Ayala, P. Y.; Morokuma, K.; Voth, G. A.; Salvador, P.; Dannenberg, J. J.; Zakrzewski, V. G.; Dapprich, S.; Daniels, A. D.; Strain, M. C.; Farkas, O.; Malick, D. K.; Rabuck, A. D.; Raghavachari, K.; Foresman, J. B.; Ortiz, J. V.; Cui, Q.; Baboul, A. G.; Clifford, S.; Cioslowski, J.; Stefanov, B. B.; Liu, G.; Liashenko, A.; Piskorz, P.; Komaromi, I.; Martin, R. L.; Fox, D. J.; Keith, T.; Al-Laham, M. A.; Peng, C. Y.; Nanayakkara, A.; Challacombe, M.; Gill, P. M. W.; Johnson, B.; Chen, W.; Wong, M. W.; Gonzalez, C.; Pople, J. A. *Gaussian 03*, revision D.01; Gaussian, Inc.: Wallingford, CT, 2005).

*2. Synthesis of **PyCh***

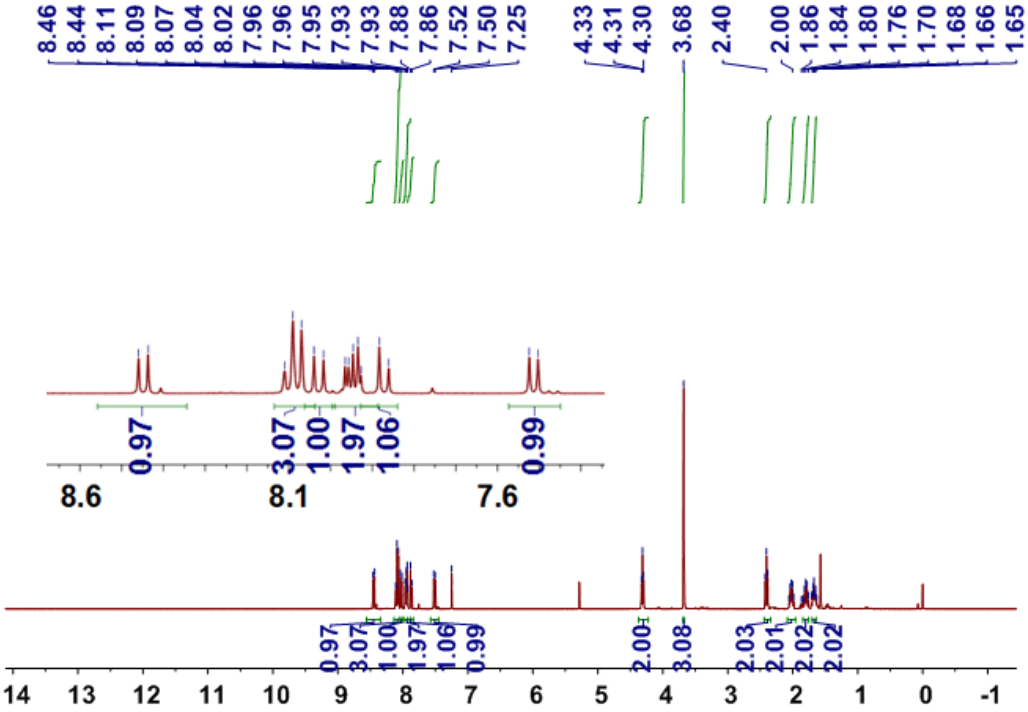


**Fig. S1** $^{1}$H NMR spectrum (400 MHz, chloroform-*d*, room temperature) of **1**.

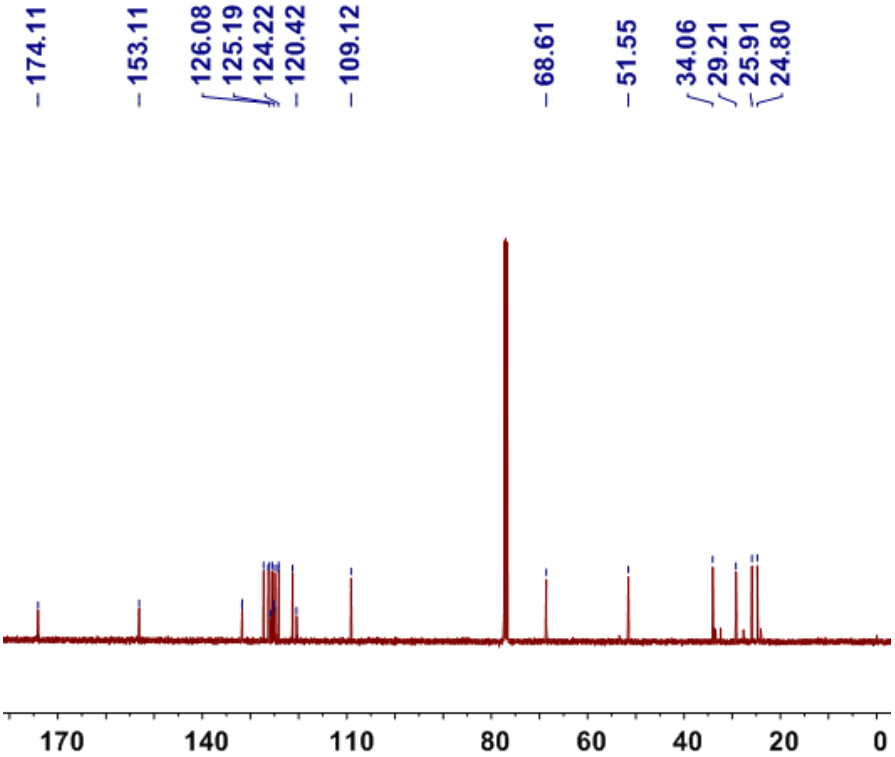


**Fig. S2** $^{13}$C NMR spectrum (100 MHz, chloroform-*d*, room temperature) of **1**.

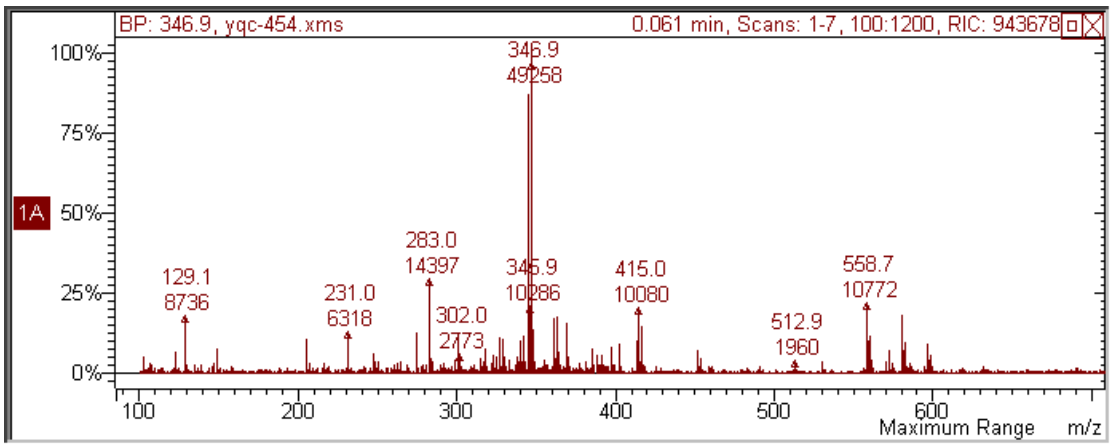


**Fig. S3** Electrospray ionization mass spectrum of **1**. Assignment of the main peak: *m/z* 346.9 [**M** + H]$^+$ (100%).

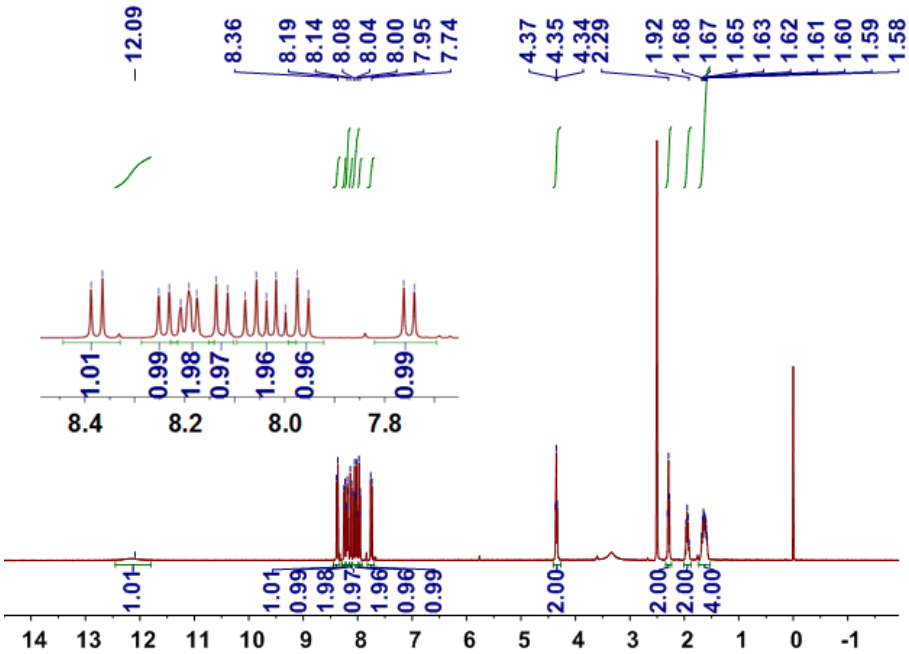


**Fig. S4** $^1$H NMR spectrum (400 MHz, DMSO-$d_6$, room temperature) of **2**.

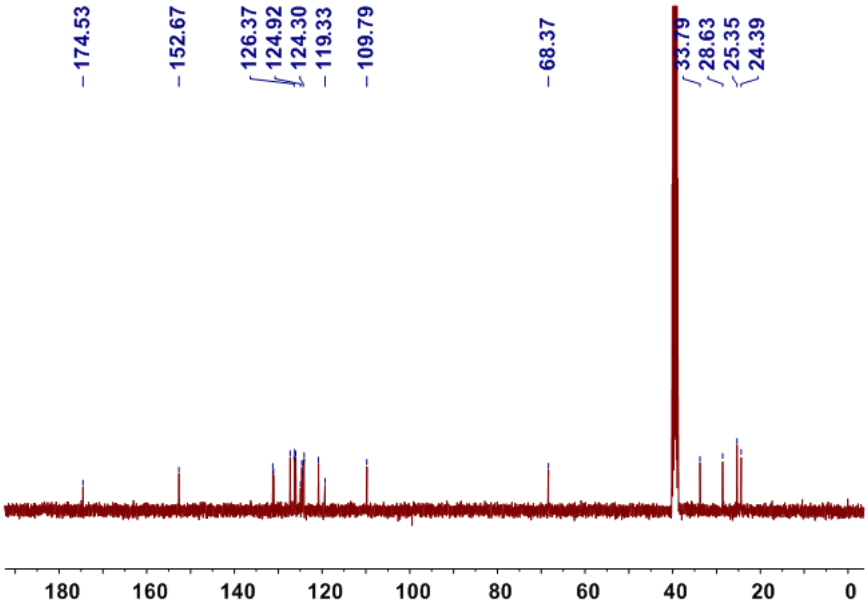


**Fig. S5** $^{13}$C NMR spectrum (100 MHz, DMSO-$d_6$, room temperature) of **2**.

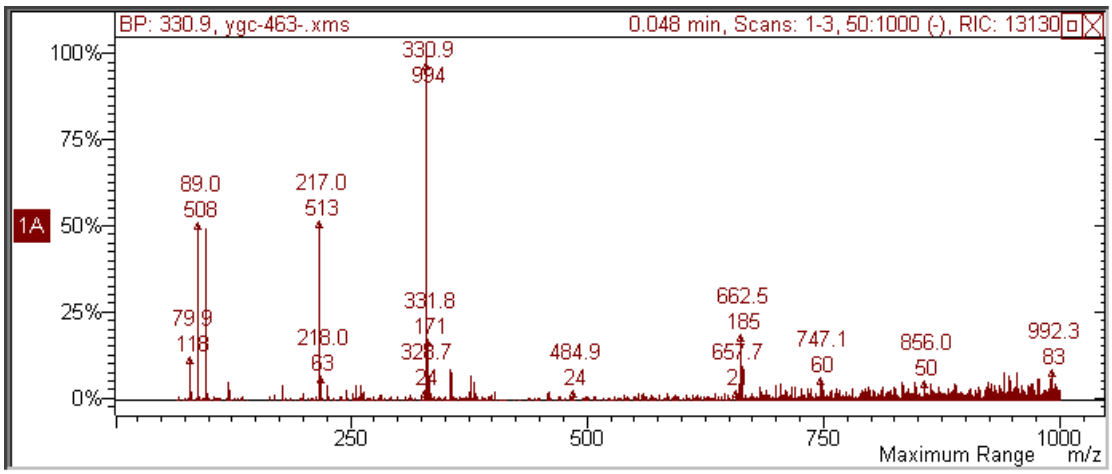


**Fig. S6** Electrospray ionization mass spectrum of **2**. Assignment of the main peak: *m*/*z* 330.9 $[M-H]^-$ (100%).

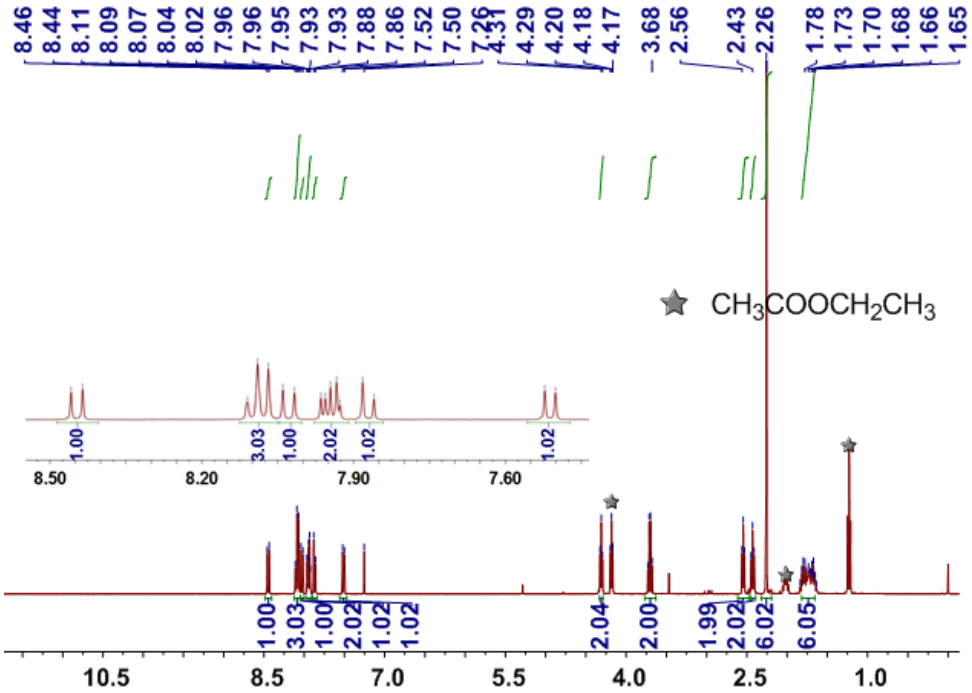


**Fig. S7** $^1$H NMR spectrum (400 MHz, chloroform-*d*, room temperature) of **3**.

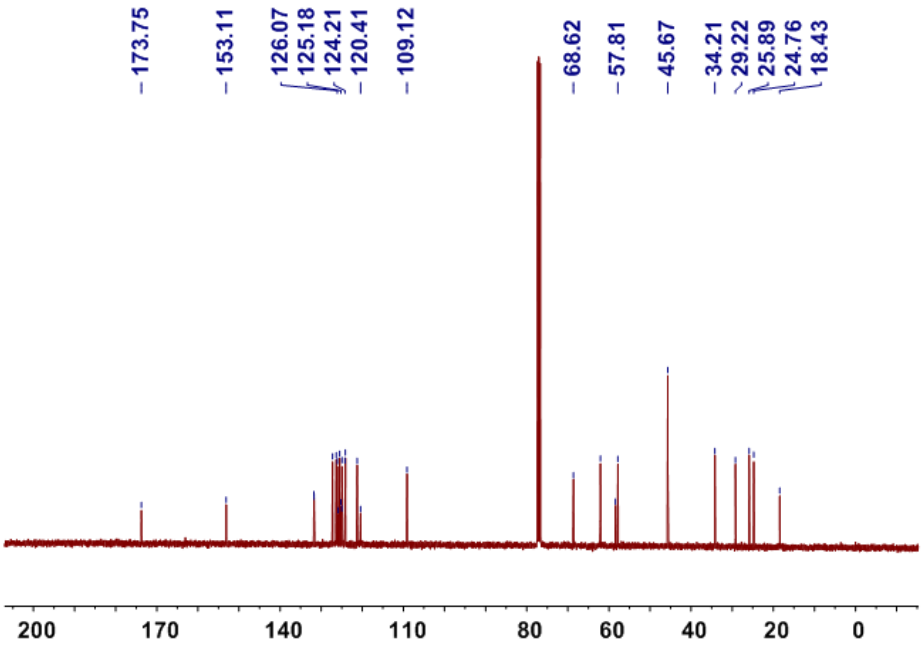


**Fig. S8** $^{13}$C NMR spectrum (100 MHz, chloroform-*d*, room temperature) of **3**.

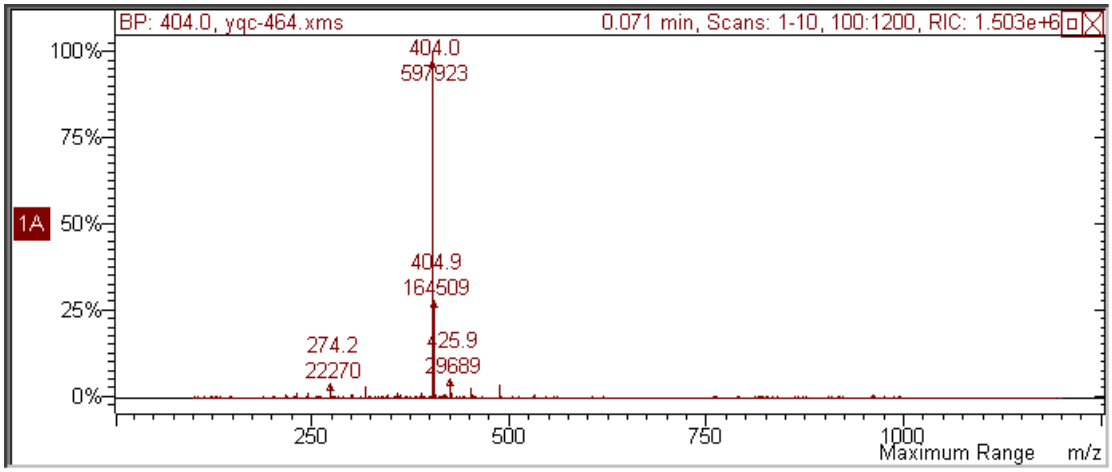


**Fig. S9** Electrospray ionization mass spectrum of **3**. Assignment of the main peak: *m/z* 404.0 $[M + H]^+$ (100%).

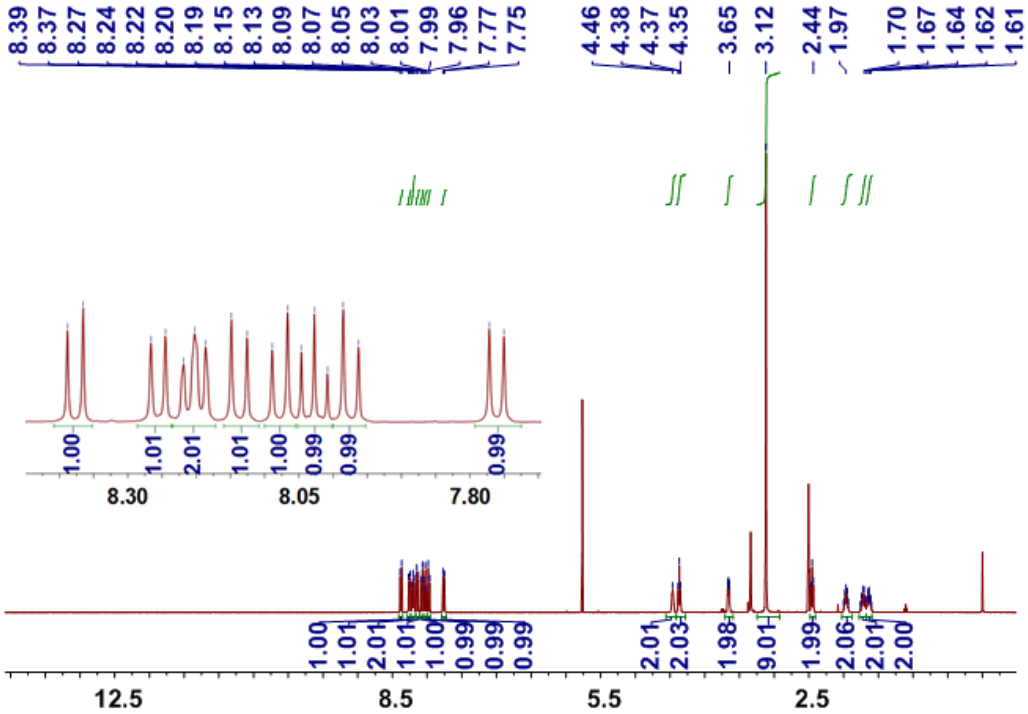


**Fig. S10** $^{1}$H NMR spectrum (400 MHz, DMSO-$d_6$, room temperature) of **PyCh**.

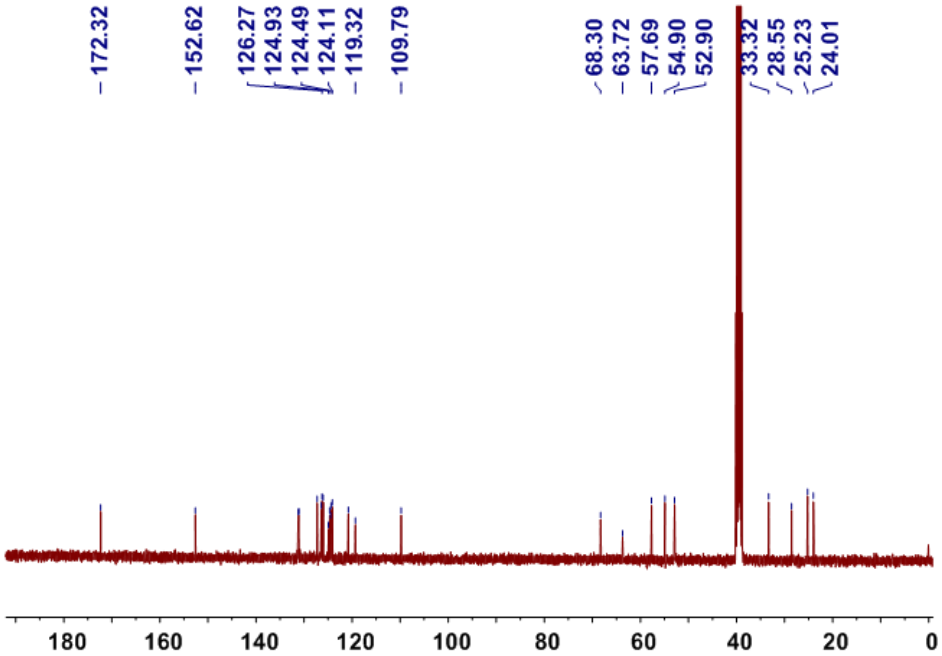


**Fig. S11** $^{13}$C NMR spectrum (100 MHz, DMSO-$d_6$, room temperature) of **PyCh**.

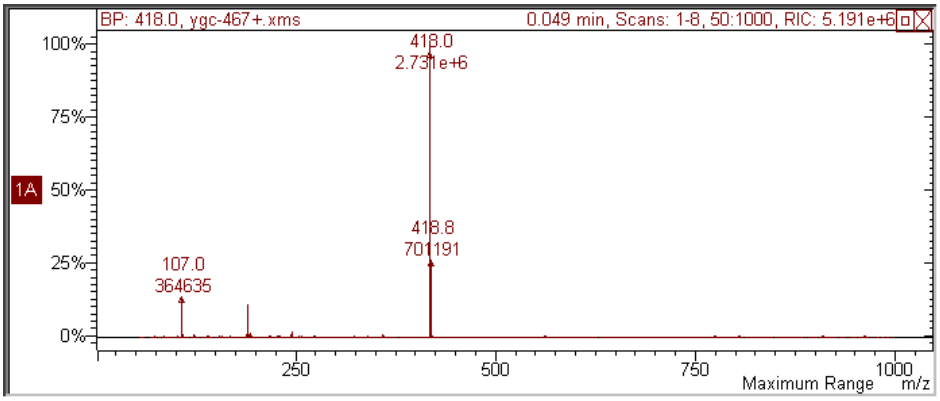


**Fig. S12** Electrospray ionization mass spectrum of **PyCh**. Assignment of the main peak: *m*/*z* 418.0 $[M - I]^+$ (100%).

*3. Host–guest complexation between **WP5** and **M***

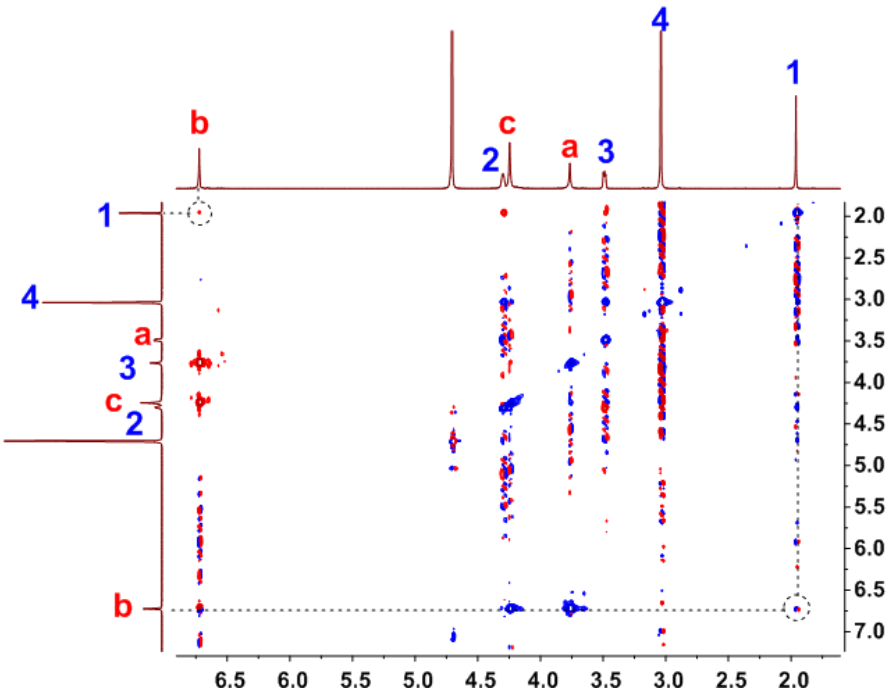


**Fig. S13** 2D NOESY NMR spectrum (500 MHz, $D_2O$, 295 K) of **WP5** (10.0 mM) and **M** (10.0 mM).

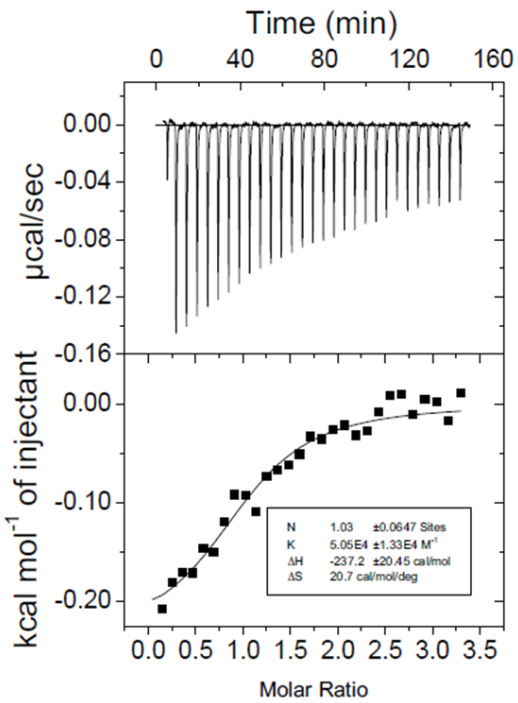


**Fig. S14** Microcalorimetric titration of **M** with **WP5** in water at 298.15 K. (Top) Raw ITC data for 29 sequential injections (10 µL per injection) of a **M** solution (2.00 mM) into a **WP5** solution (0.100 mM). (Bottom) Net reaction heat obtained from the integration of the calorimetric traces.

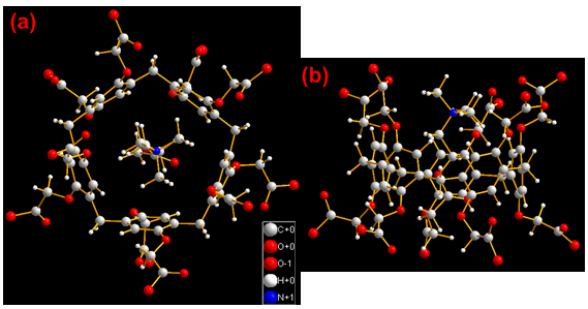


**Fig. S15** Energy-minimized structure of **WP5⊃M** by the PM3 semiempirical molecular orbital method: (a) top view, (b) side view.

*4. Host–guest complexation between **WP5** and **PyCh***

Further evidence for the formation of a stable host–guest complex **WP5⊃PyCh** was obtained from UV-vis absorption spectroscopy. When **WP5** and **PyCh** (molar ratio = 1:1) were mixed in water, a notable red-shift was observed, confirming the presence of electronic communication between **WP5** and **PyCh**.

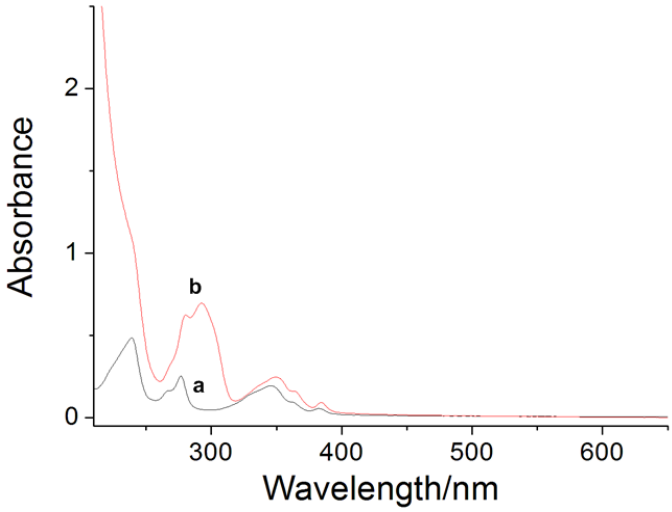


**Fig. S16** UV-vis spectra of (a) **PyCh** and (b) **WP5⊃PyCh** in water.

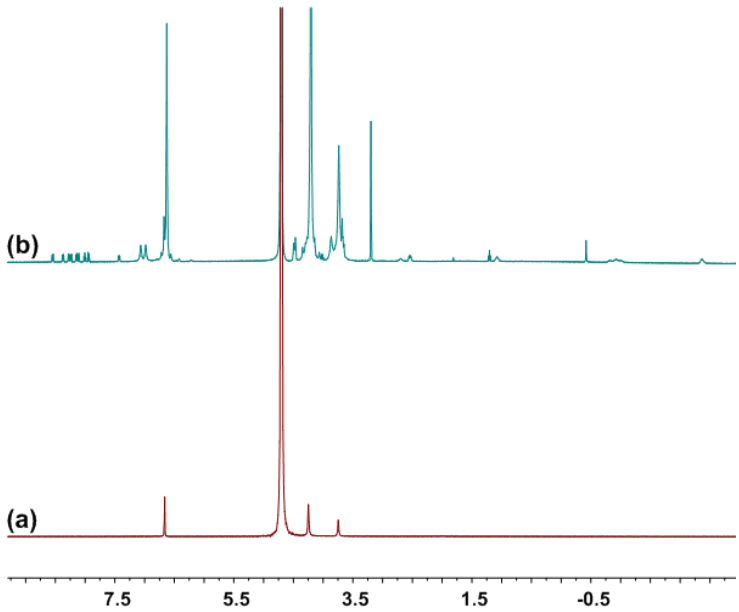


**Fig. S17** Partial $^1$H NMR spectra (400 MHz, $D_2O$, 295 K): (a) **WP5** (2.00 mM) and **PyCh** (6.00 mM); (b) **WP5** (2.00 mM).

*5. Critical aggregation concentration determination of **PyCh** and **WP5⊃PyCh***

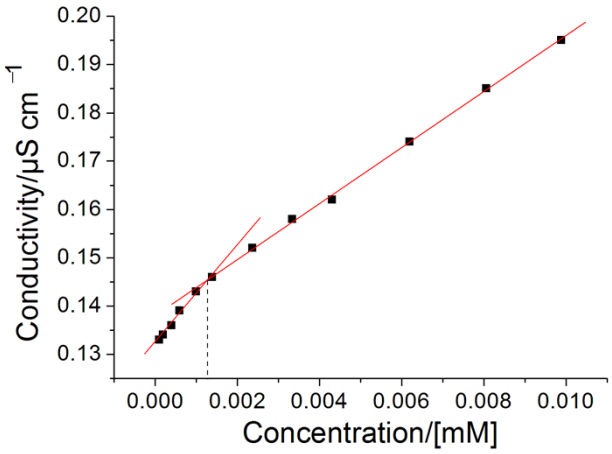


**Fig. S18** The concentration-dependent conductivity of **PyCh**. The critical aggregation concentration was determined to be $1.25 \times 10^{-6}$ M.

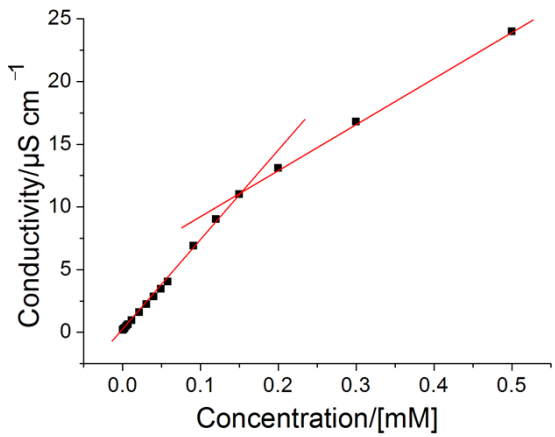


**Fig. S19** The concentration-dependent conductivity of **WP5⊃PyCh**. The critical aggregation concentration was determined to be $1.52 \times 10^{-4}$ M.

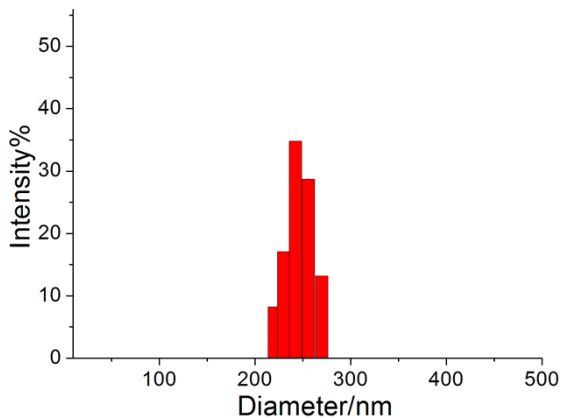


**Fig. S20** DLS result of the nanoparticles formed by **WP5⊃PyCh**.

*6. Packing mode investigation of **PyCh** before and after treating with AChE*

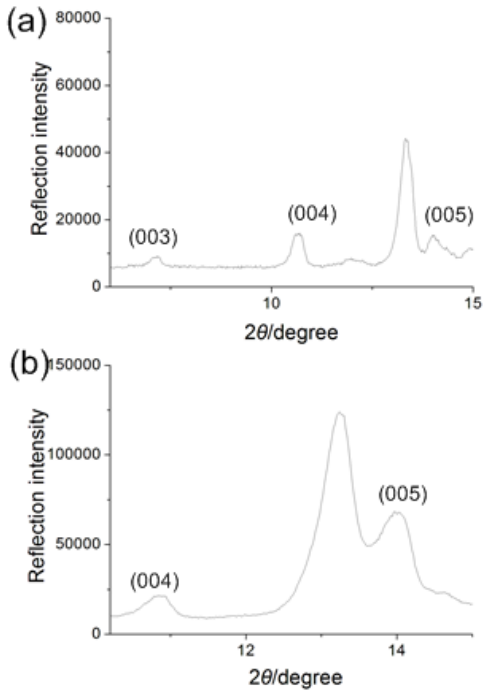


**Fig. S21** XRD scans of (a) nanosheets and (b) nanoribbons.

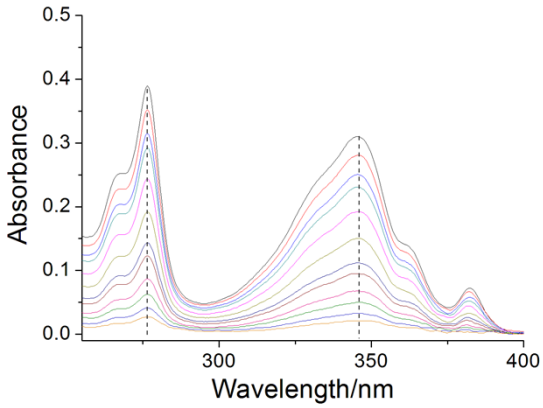


**Fig. S22** UV−vis absorption spectra of aqueous solutions of **PyCh** at different concentrations.

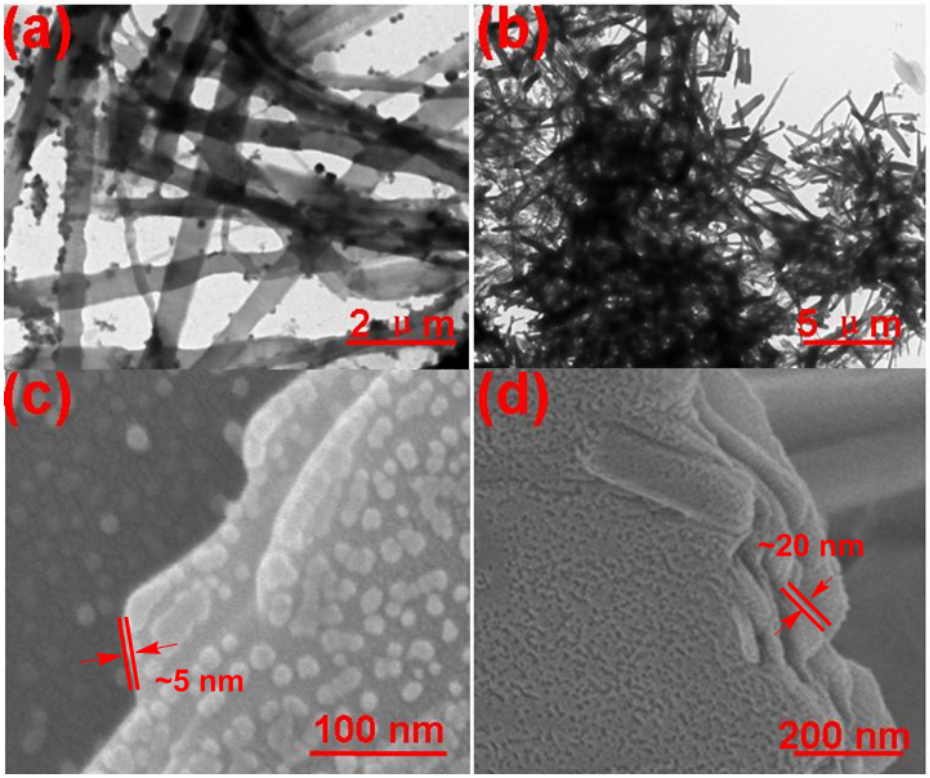


**Fig. S23** TEM images of (a) the intermediate state from nanoparticles to nanoribbons, (b) **PyCh** treated with AChE, (c) nanosheets formed by **PyCh**, and (d) multilayer nanorribons.

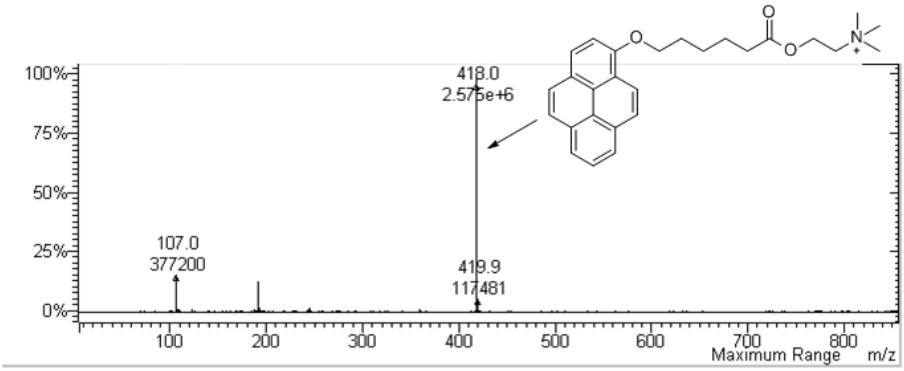


**Fig. S24** Electrospray ionization mass spectrum of **PyCh** in the absence of AChE.

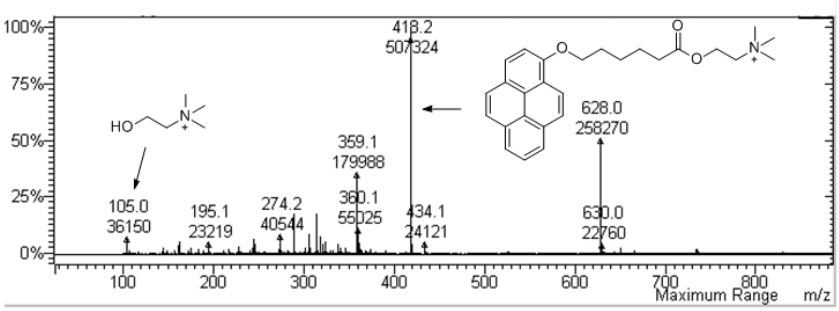


**Fig. S25** Electrospray ionization mass spectrum of **PyCh** after treatment with AChE for 5 h.

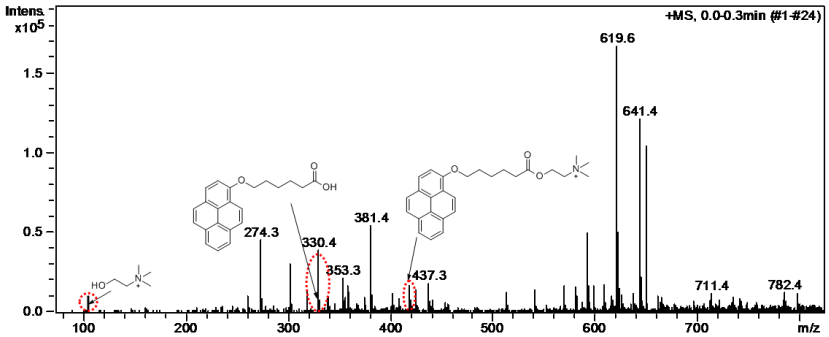


**Fig. S26** Electrospray ionization mass spectrum of **PyCh** after treatment with AChE for 12 h.

*7. Preparation of supramolecular hybrid materials*

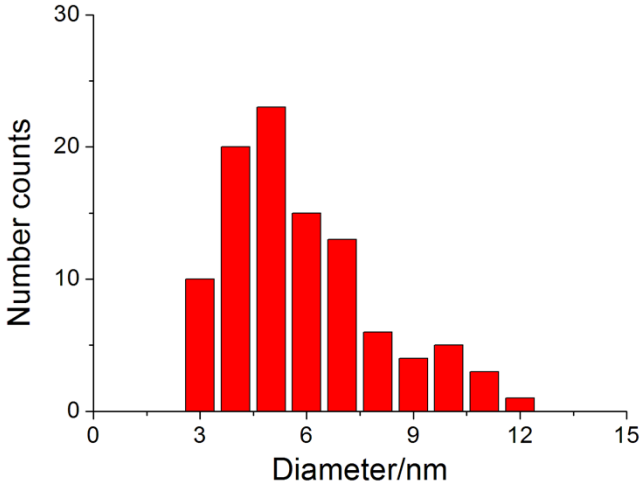


**Fig. S27** Size histogram of gold nanoparticles corresponding to the hybrid AuNPs@nanosheets based on 100 particles.

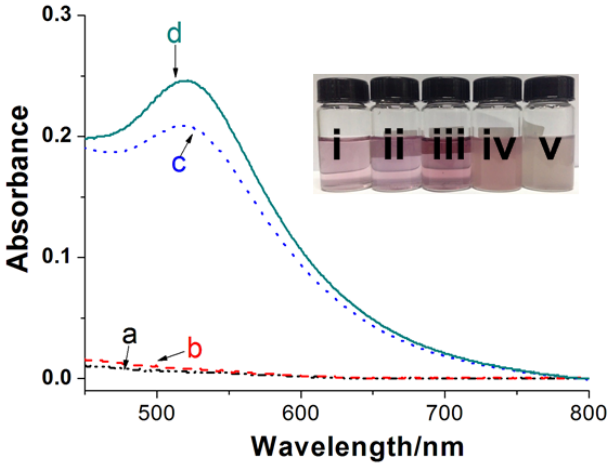


**Fig. S28** UV-vis spectra of (a) **PyCh**, (b) **WP5⊃PyCh**, (c) AuNPs@nanosheets, and (d) AuNPs@particles. Inset: i, AuNPs@nanoparticles after treating with AChE; ii, AuNPs@nanoparticles; iii, AuNPs; iv, AuNPs@nanosheets; v, AuNPs@nanosheets after treating with AChE.

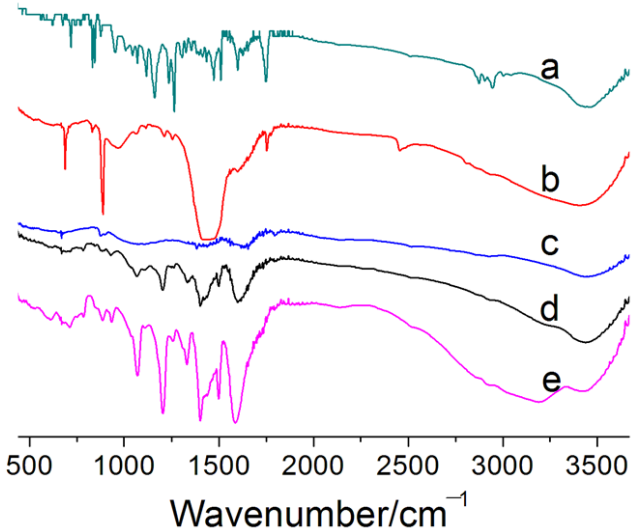


**Fig. S29** Fourier transform IR spectra of (a) **PyCh**, (b) Au@nanosheets, (c) bare AuNPs, (d) Au@nanoparticles and (e) **WP5**.

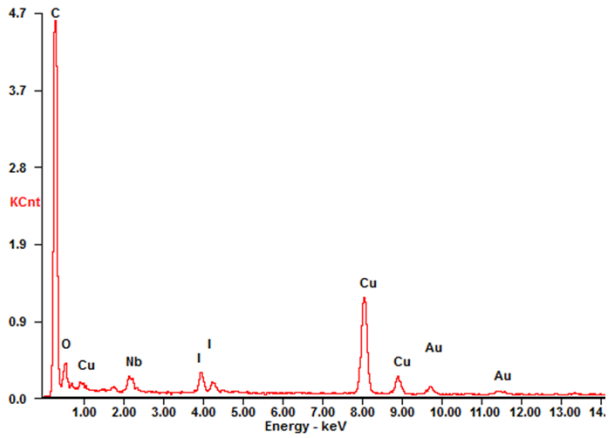


**Fig. S30** EDS study of the Au@nanosheets.

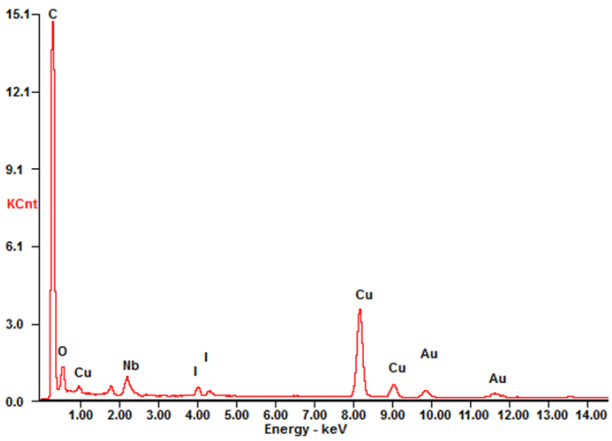


**Fig. S31** EDS study of the Au@nanoparticles.

*8. Catalytic reduction of 4-nitroanilin*

In our reaction system, the concentration of $BH_4^-$ greatly exceeded that of 4-nitroaniline, so it is reasonable to consider its concentration to be constant during the reaction. As expected, a good linear correlation of ln(A) versus time was obtained, and the kinetic reaction rate constant was estimated.[S1]

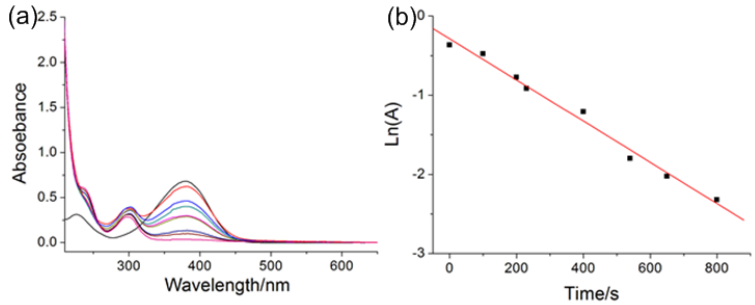


**Fig. S32** (a) The successive UV-vis absorption of the reduction of 4-nitroaniline and (b) plot of ln(A) against time with excess $NaBH_4$ in the presence of Au@nanoparticles. The kinetic reaction rate constant was calculated to be $(2.61 \pm 0.28) \times 10^{-3}$ $S^{-1}$.

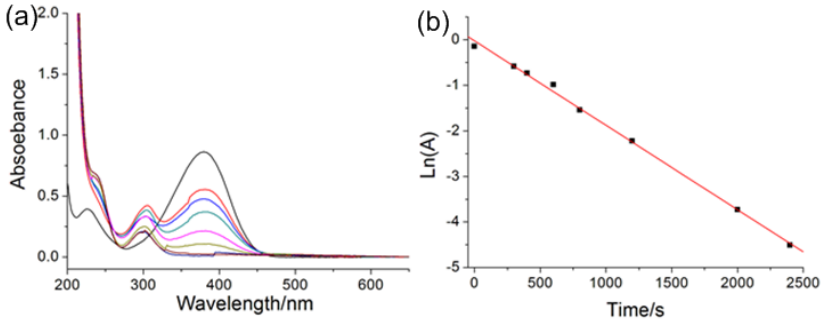


**Fig. S33** (a) The successive UV-vis absorption of the reduction of 4-nitroaniline and (b) plot of ln(A) against time with excess $NaBH_4$ in the presence of Au@nanosheets. The kinetic reaction rate constant was calculated to be $(1.85 \pm 0.15) \times 10^{-3}$ $S^{-1}$.

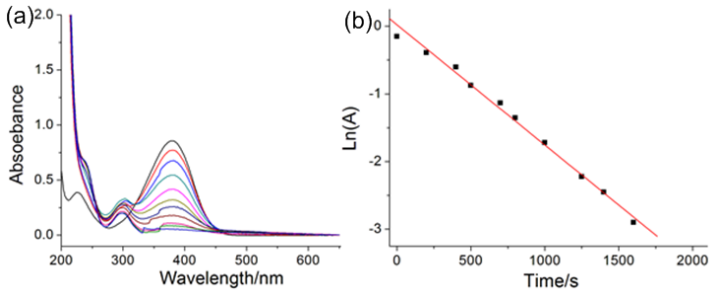


**Fig. S34** (a) The successive UV-vis absorption of the reduction of 4-nitroaniline and (b) plot of ln(A) against time with excess $NaBH_4$ in the presence of Au@nanoparticles after treatment with AChE. The kinetic reaction rate constant was calculated to be $(1.78 \pm 0.11) \times 10^{-3}$ $S^{-1}$.

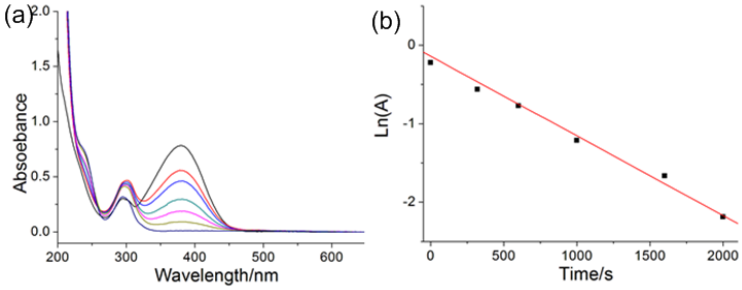


**Fig. S35** (a) The successive UV-vis absorption of the reduction of 4-nitroaniline and (b) plot of ln(A) against time with excess $NaBH_4$ in the presence of Au@nanosheets after treatment with AChE. The kinetic reaction rate constant was calculated to be $(1.01 \pm 0.09) \times 10^{-3}$ $S^{-1}$.

*References*:

S1. (a) Yao, Y.; Xue, M.; Chi, X.; Ma, Y.; He, J.; Abliz, Z.; Huang, F. *Chem. Commun*. **2012**, *48*, 6505–6507; (b) Yao, Y.; Xue, M.; Zhang, Z.; Zhang, M.; Wang, Y.; Huang, F. *Chem. Sci*. **2013**, *4*, 3667–3672.